largest absolute correlations with the label. However, he or she verifies the correlations (with the label) on the holdout set and uses only those variables whose correlation agrees in sign with the correlation on the training set and for which both correlations are larger than some threshold in absolute value. The analyst then creates a simple linear threshold classifier on the selected variables using only the signs of the correlations of the selected variables. A final test evaluates the classification accuracy of the classifier on the holdout set. Full details of the analyst's algorithm can be found in section 3 of (*17*).

In our first experiment, each attribute is drawn independently from the normal distribution $N(0,1)$, and we choose the class label $y \in \{-1, 1\}$ uniformly at random so that there is no correlation between the data point and its label. We chose $n = 10,000$ and $d = 10,000$ and varied the number of selected variables k. In this scenario no classifier can achieve true accuracy better than 50%. Nevertheless, reusing a standard holdout results in reported accuracy of $>63 \pm 0.4\%$ for $k = 500$ on both the training set and the holdout set. The average and standard deviation of results obtained from 100 independent executions of the experiment are plotted in Fig. 1A, which also includes the accuracy of the classifier on another fresh data set of size n drawn from the same distribution. We then executed the same algorithm with our reusable holdout. The algorithm Thresholdout was invoked with $T = 0.04$ and $\tau = 0.01$, which explains why the accuracy of the classifier reported by Thresholdout is off by up to 0.04 whenever the accuracy on the holdout set is within 0.04 of the accuracy on the training set. Thresholdout prevents the algorithm from overfitting to the holdout set and gives a valid estimate of classifier accuracy. In Fig. 1B, we plot the accuracy of the classifier as reported by Thresholdout. In addition, in fig. S2 we include a plot of the actual accuracy of the produced classifier on the holdout set.

In our second experiment, the class labels are correlated with some of the variables. As before, the label is randomly chosen from $\{-1,1\}$ and each of the attributes is drawn from $N(0,1)$, aside from 20 attributes drawn from $N(y \cdot 0.06, 1)$, where y is the class label. We execute the same algorithm on this data with both the standard holdout and Thresholdout and plot the results in Fig. 2. Our experiment shows that when using the reusable holdout, the algorithm still finds a good classifier while preventing overfitting.

Overfitting to the standard holdout set arises in our experiment because the analyst reuses the holdout after using it to measure the correlation of single attributes. We first note that neither cross-validation nor bootstrap resolve this issue. If we used either of these methods to validate the correlations, overfitting would still arise as a result of using the same data for training and validation (of the final classifier). It is tempting to recommend other solutions to the specific problem on which we based our experiment. Indeed, a substantial number of methods in the statistics literature deal with inference for fixed two-step

procedures in which the first step is variable selection [see (*5*) for examples]. Our experiment demonstrates that even in such simple and standard settings, our method avoids false discovery without the need to use a specialized procedure and, of course, extends more broadly. More importantly, the reusable holdout gives the analyst a general and principled method to perform multiple validation steps where previously the only known safe approach was to collect a fresh holdout set each time a function depends on the outcomes of previous validations.

REFERENCES AND NOTES

1. Y. Benjamini, Y. Hochberg, *J. R. Stat. Soc. B* **57**, 289–300 (1995).
2. J. P. A. Ioannidis, *PLOS Med.* **2**, e124 (2005).
3. J. P. Simmons, L. D. Nelson, U. Simonsohn, *Psychol. Sci.* **22**, 1359–1366 (2011).
4. A. Gelman, E. Loken, *Am. Stat.* **102**, 460 (2014).
5. T. Hastie, R. Tibshirani, J. H. Friedman, *The Elements of Statistical Learning: Data Mining, Inference, and Prediction* (Springer Series in Statistics, Springer, New York, ed. 2, 2009).
6. D. Foster, R. Stine, *J. R. Stat. Soc. B* **70**, 429–444 (2008).
7. E. Aharoni, H. Neuvirth, S. Rosset, *IEEE/ACM Trans. Comput. Biol. Bioinform.* **8**, 1431–1437 (2011).
8. J. Javanmard, A. Montanari, On online control of false discovery rate. http://arxiv.org/abs/1502.06197 (2015).
9. C. Chambers, M. Munafo, "Trust in science would be improved by study pre-registration," *Guardian US*, 5 June 2013; www.theguardian.com/science/blog/2013/jun/05/trust-in-science-study-pre-registration.
10. J. Reunanen, *J. Mach. Learn. Res.* **3**, 1371–1382 (2003).
11. R. B. Rao, G. Fung, in *Proceedings of the SIAM International Conference on Data Mining 2008* (Society for Industrial and Applied Mathematics, Philadelphia, PA, 2008), pp. 588–596.
12. G. C. Cawley, N. L. C. Talbot, *J. Mach. Learn. Res.* **11**, 2079–2107 (2010).
13. C. Dwork, F. McSherry, K. Nissim, A. Smith, in *Theory of Cryptography* (Lecture Notes in Computer Science Series, Springer, Berlin, 2006), pp. 265–284.
14. O. Bousquet, A. Elisseeff, *J. Mach. Learn. Res.* **2**, 499–526 (2002).
15. T. Poggio, R. Rifkin, S. Mukherjee, P. Niyogi, *Nature* **428**, 419–422 (2004).
16. S. Shalev-Shwartz, O. Shamir, N. Srebro, K. Sridharan, *J. Mach. Learn. Res.* **11**, 2635–2670 (2010).
17. Supplementary materials are available on *Science* Online.
18. D. A. Freedman, *Am. Stat.* **37**, 152–155 (1983).

ENVIRONMENTAL SCIENCE

Profiling risk and sustainability in coastal deltas of the world

Z. D. Tessler,[1]* C. J. Vörösmarty,[1,2] M. Grossberg,[3] I. Gladkova,[3] H. Aizenman,[3] J. P. M. Syvitski,[4] E. Foufoula-Georgiou[5]

Deltas are highly sensitive to increasing risks arising from local human activities, land subsidence, regional water management, global sea-level rise, and climate extremes. We quantified changing flood risk due to extreme events using an integrated set of global environmental, geophysical, and social indicators. Although risks are distributed across all levels of economic development, wealthy countries effectively limit their present-day threat by gross domestic product–enabled infrastructure and coastal defense investments. In an energy-constrained future, such protections will probably prove to be unsustainable, raising relative risks by four to eight times in the Mississippi and Rhine deltas and by one-and-a-half to four times in the Chao Phraya and Yangtze deltas. The current emphasis on short-term solutions for the world's deltas will greatly constrain options for designing sustainable solutions in the long term.

Deltas present a quintessential challenge for humans amid global environmental change. Home to some of the world's largest urban areas, deltas are also highly dynamic landforms shaped by fluvial and coastal flooding (*1–3*). Human activities at the local and regional scales can perturb the water and sedimentary dynamics necessary to maintain a delta's integrity, increasing the rate of relative sea-level rise (RSLR, the combination of land subsidence and offshore sea-level rise) and increasing flood risk (*4, 5*).

Delta sediments naturally compact over time, requiring new sediment fluxes from the upstream river network and deposition on the delta surface

[1]Environmental CrossRoads Initiative, City University of New York, NY 10031, USA. [2]Department of Civil Engineering, City College of New York, New York, NY 10031, USA. [3]Department of Computer Science, City College of New York, NY 10031, USA. [4]Department of Geological Sciences, University of Colorado–Boulder, Boulder, CO 80309, USA. [5]Department of Civil, Environmental, and Geo- Engineering, University of Minnesota, Minneapolis, MN 55455, USA.
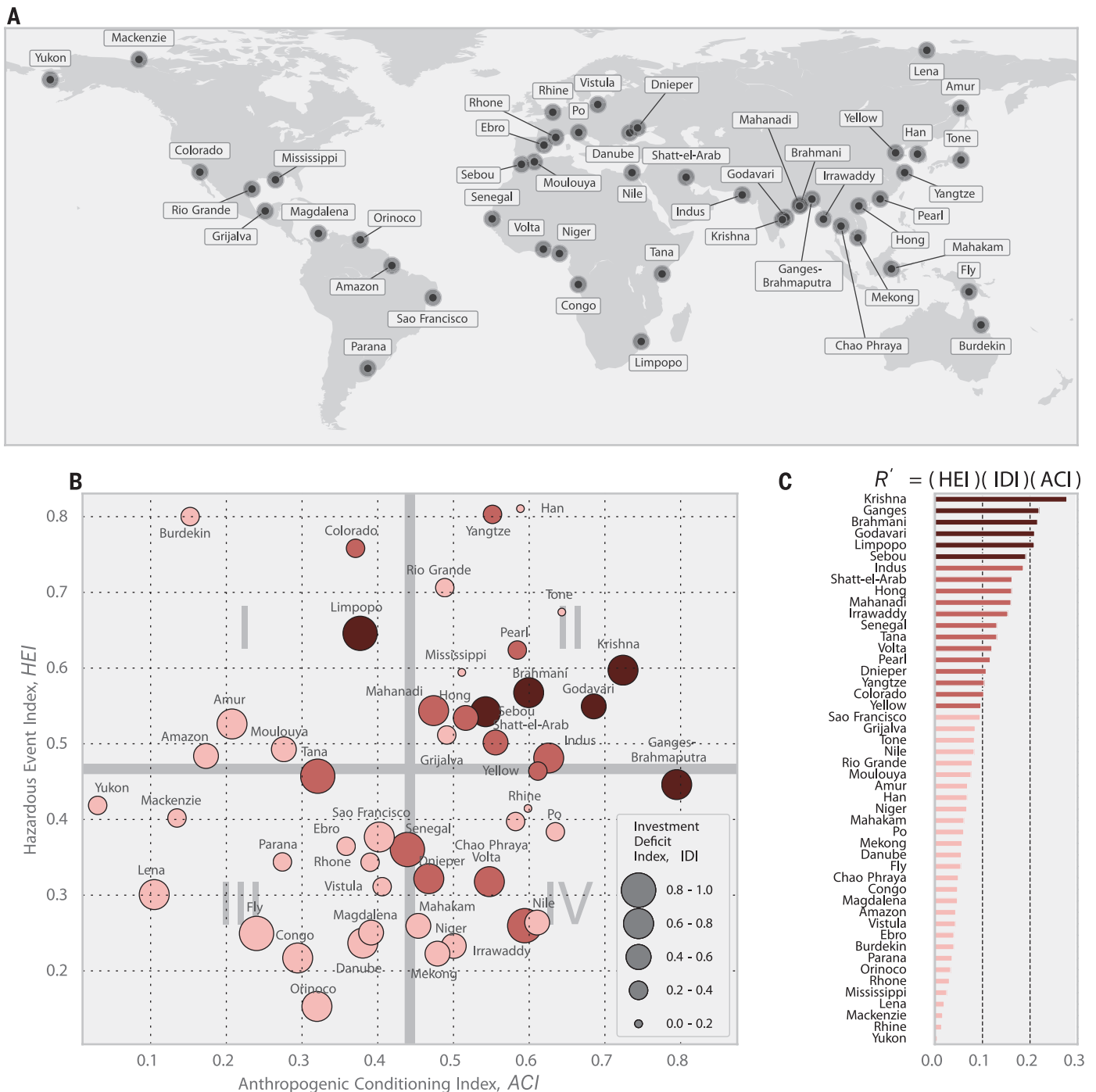*Corresponding author. E-mail: ztessler@ccny.cuny.edu

to maintain land elevation (4). Upstream dams and reservoirs trap sediment (6), and soil conservation practices can reduce the mobilization of sediment (7). River channelization on deltas inhibits depositional processes (8), whereas urban construction and groundwater extraction can accelerate sediment compaction (9, 10). Land subsidence is compounded by rising sea levels and the changing intensity and distribution of extreme events related to climate change (11, 12). Policies aimed at reducing the apparent levels of risk often employ costly engineering solutions that may be inherently unsustainable (13–15). A framework to enable comparative risk assessment for deltas across the globe that specifically accounts for the dual natural and anthropogenic forces shaping these systems is a necessary precursor for strategies to improve their long-term resilience (16).

We present a systematic global-scale assessment of the changing risk profiles of coastal deltas. Most manifestations of risk are the immediate

Fig. 1. Risk trends for deltas worldwide. (**A**) Map showing the 48 deltas included in this study. (**B**) Phase diagram of contemporary risk assessment results, showing the three component proxy indices used to estimate per-capita R'. Color density represents a delta's overall risk trend. Quadrant III deltas have predominantly low R', whereas quadrant II deltas have high R'. (**C**) Estimates of the relative rate of change in risk, or risk trend, for each delta due to increasing exposure associated with RSLR. The Krishna and Ganges-Brahmaputra deltas, despite being only moderately susceptible to short-term hazardous events, are increasingly at risk because of high rates of RSLR and high socioeconomic vulnerability. Ganges-Brahmaputra is abbreviated to "Ganges" in some panels for brevity.

consequences of extreme events (*3*), such as fluvial and coastal flooding, that act over short time scales. Overall risk, however, is conditioned over longer periods by anthropogenically modified geomorphic processes such as changes in sediment supply, deposition, and compaction—which increase land subsidence and RSLR—and by the socioeconomic capability to prepare for and mitigate exposure to hazardous conditions (*17*). Focusing on interdelta differences in risk, we used sufficiently mature global data sets that depict factors with well-documented impacts on delta conditions, together with established methods for spatial integration of qualitatively distinct data types (*18–20*). We focused on 48 major coastal deltas across a wide range of climate, biome, and socioeconomic contexts (Fig. 1A), with an estimated current combined population of over 340 million (*21*) (see the supplementary materials). At less direct risk are an additional 140 million people living within 25 km of these deltas, who, together with 3.5 billion people in upstream catchment basins, produce additional human impacts. We defined risk (*R*), or expected loss, to a delta population as a product of hazard (*H*), exposure (*E*), and vulnerability (*V*): $R = HEV$ (*17, 22, 23*). Hazard is the probability of a damage-producing event, defined as fluvial or coastal flooding. Exposure is the expected number of people exposed to hazardous conditions for a given event, and vulnerability is the harm or loss caused by the exposure (eq. S1).

Previous direct estimates of *H*, *E*, and *V* have been carried out in a number of local and regional studies (*23–25*) using high-resolution data sets that are not currently available at the global scale. Exposure data at the necessary scales exist for select deltas; however, for global-scale analysis, the rate of change in exposure, *E'*, is a more tractable measure for interdelta comparison. By reducing the relative elevation of a delta, RSLR results in increased population exposure to a given hazard and thus increased expected loss. The rate of change in expected loss (*R'*) due to anthropogenic RSLR is termed the risk trend: $R' = HE'V$ (see the supplementary materials).

We estimated *H*, *E'*, and *V* for each delta, using empirical indices derived from global data sets. The Hazardous Event Index (HEI) is a proxy for hazard, based on empirical indicators of the probability and intensity of delta flood events. *E'* was estimated using the Anthropogenic Conditioning Index (ACI), which is built from measures of long-term anthropogenic drivers of RSLR (fig. S1). Vulnerability, which is strongly dependent on socioeconomic conditions in the delta (*17, 22*), was estimated as a function of per-capita gross domestic product (GDP), aggregate GDP, and government effectiveness. High GDP provides the financial capacity to make vulnerability-reducing investments from household to delta scales, when effective governments are present to leverage aggregate wealth to reduce vulnerability. An

index representing the absence of this capacity, the Investment Deficit Index (IDI), was used as a proxy for *V*. The risk component estimates derived from the ACI, HEI, and IDI indices were used to estimate the risk trend resulting from RSLR (eq. S7).

We mapped the 48 deltas into a risk space defined by each delta's specific anthropogenic, geophysical, and socioeconomic characteristics (Fig. 1). These estimates were made in an index space, comparing delta systems with each other on a relative per-capita basis. In quadrant I, which contains deltas with low ACI and high HEI scores, the Limpopo delta stands out because of its high vulnerability associated with a lack of infrastructure investment capacity. Most of the high-*R'* deltas fell in quadrant II, including the Krishna delta, which had the highest *R'*. In quadrant IV, characterized by high ACI and low to moderate HEI scores, the Ganges-Brahmaputra delta had a high *R'* due to high vulnerability. In contrast, quadrant III contains deltas with low *R'* due to both low ACI and low HEI scores, including the high-latitude Yukon, Lena, and Mackenzie deltas.

The Mississippi, Rhine, and Tone deltas had ACI and HEI scores similar to those of the Brahmani and Godavari deltas (between 0.4 and 0.7), but they had far lower IDI scores (<0.2). Their resulting risk levels were much more stable, with risk trends among the lowest of all the deltas in the study. Although the results presented here
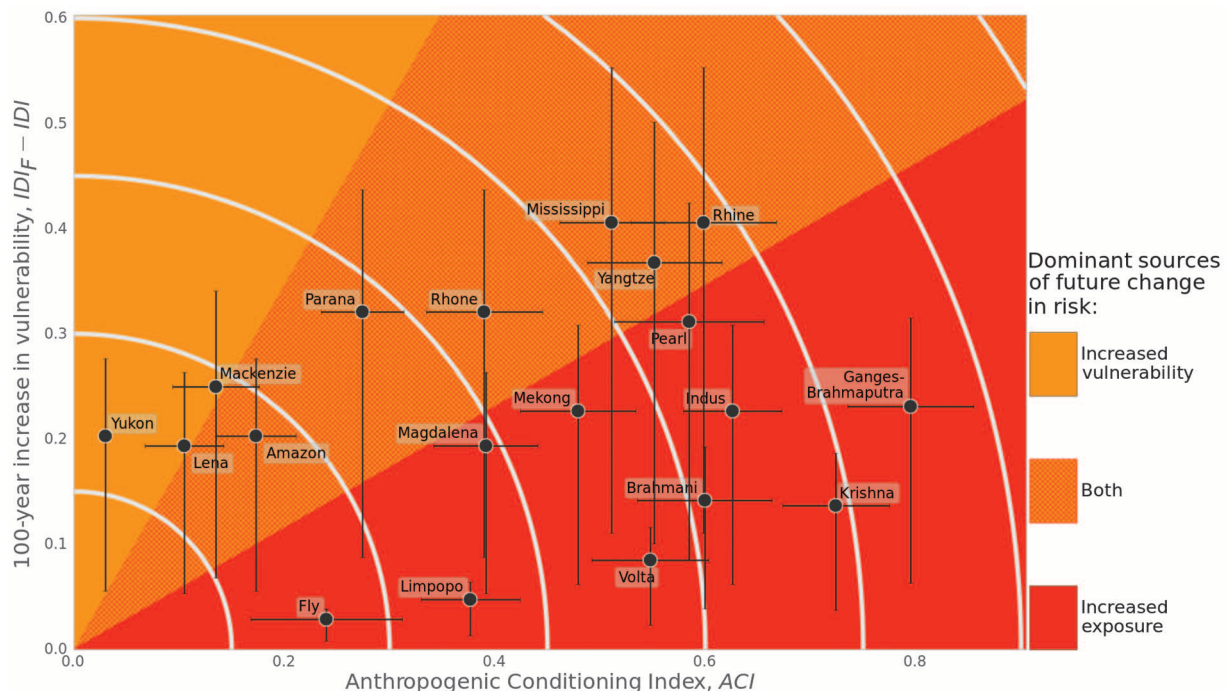

Fig. 2. Estimated future change in exposure and vulnerability for selected deltas. The vertical axis, showing one scenario of change in vulnerability, is the difference between the 100-year future Investment Deficit Index, IDI_F, and the current index, IDI. The origin represents current conditions. Both axes indicate a change over time for the two risk components: Increases in exposure are taken as proportional to the current rate of change, and increases in vulnerability are based on the difference between current and future estimates. Future change in risk is either associated predominately with increases in exposure (red) or increases in vulnerability (orange). Several delta systems (e.g., Mississippi, Rhine, and Yangtze) are at risk both from RSLR, leading to increased exposure to flooding, and from reduced effectiveness of risk reduction strategies that may not be sustainable on the century scale.

are for per-capita risk, the Ganges-Brahmaputra system had, by far, the greatest rate of change in risk when aggregating across delta populations. The Ganges-Brahmaputra had the second highest R' on a per-capita basis, and at more than 100 million people, it has more than twice the population of the Nile, the second most populous delta.

A low IDI, indicating a high capacity for investment in risk-reducing technologies, is the primary reason that several wealthy, developed deltas today have relatively low risk trends. For instance, after catastrophic flooding of the Rhine delta in 1953, the Dutch Delta Works were constructed to reduce future flood risk, using a network of storm-surge barriers, dams, levees, and other engineered structures. A long history of land subsidence, however, has left parts of this delta 6 m below sea level (26). Modernization and improvement costs across the Netherlands are projected to reach €1 billion to €2

billion per annum over the next century (27). The long-term sustainability of this and similar risk-reducing investments elsewhere has been called into question because of their heavy reliance on external financial and energy subsidies (14).

To examine the sensitivity of delta risk to reduced infrastructure investment benefits, we considered a future scenario in which infrastructure costs have increased. For our analysis, we used an increase in energy prices as a likely reason for a rise in the cost of infrastructure, but factors such as relative increases in the costs of labor and material or rising interest rates would have similar impacts on infrastructure cost. We modeled this scenario by adjusting IDI scores: We reduced GDP indicator weights based on 100-year projections of energy price growth in excess of GDP (28) (see the supplementary materials), reflecting expectations of higher costs for a given level of risk reduction. Estimates of future vulnerability increased for all deltas under

this scenario (Fig. 2) but were greatest for systems with high GDP. The Mississippi, Rhine, Han, Chao Phraya, and Yangtze deltas had the greatest increases in vulnerability under this scenario, although others were also strongly affected, including the Parana, Rhone, and Pearl deltas. Deltas in low-GDP regions, such as the Irrawaddy, Tana, and Fly, were the least sensitive to these potential future changes. These and other less economically developed deltas were instead more sensitive to future risk increases stemming from increased exposure to hazardous events.

A given increase in vulnerability will not affect risk trends in all deltas equally; rather, its effect will be related to each delta's ACI and HEI scores. We started with each system's uncompensated R' based on anthropogenic and geophysical considerations alone (Fig. 3A). When considering contemporary vulnerability estimates (Fig. 3B), the wealthy but otherwise at-risk deltas such as the Rhine, Mississippi, and Han benefited
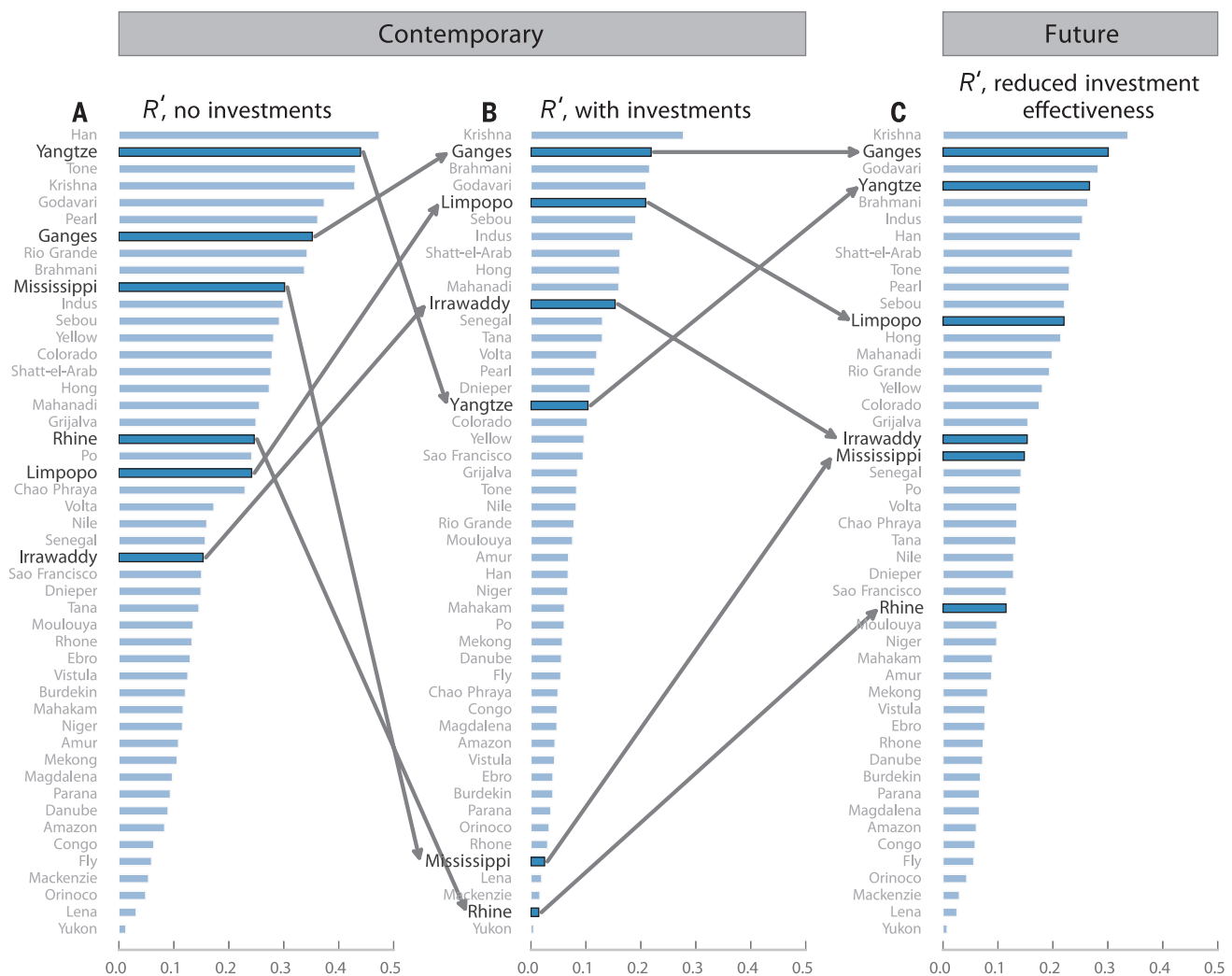

Fig. 3. Current and future investment impacts on risk-trend rankings. (A) Contemporary risk trend when considering only the anthropogenic and geophysical setting of each delta. **(B)** When also considering relative vulnerability, which is low for deltas that can make risk-reducing investments, the overall contemporary risk trend changes, in many cases dramatically. The Mississippi and Rhine deltas show substantially reduced risk. **(C)** Current risk-reduction strategies become more expensive and less sustainable in a more energy-constrained future scenario (14). In the long term, deltas that today are protected by substantial compensating infrastructure are likely to see their risk profiles approach those in (A).

substantially from their capacity to sustain engineering and infrastructure investments. Low-GDP deltas that are not able to make risk-reduction investments moved to higher risk rankings. The largest increases in R' ranks occurred for the Limpopo and Irrawaddy deltas. Improved economic development and associated vulnerability reductions would result in the largest decreases in risk in these deltas, akin to a transition from Fig. 3B to Fig. 3A. In the future vulnerability scenario (Fig. 3C), where investment capacity less effectively reduces risk trends, R' ranks for high-GDP deltas reverted back toward expectations based on geophysical hazards and anthropogenic change alone. Although contemporary estimates of risk trends were highest in South Asia (Fig. 4A), future increases in R', relative to current estimates, were greatest in the Rhine, Mississippi, Han, Tone, Chao Phraya, and Yangtze deltas (Fig. 4B). These systems are highly stressed by anthropogenic activ-

ities and regularly contend with hazardous events, so future increases in vulnerability will have a disproportionately large risk impact relative to other deltas. Management strategies that address the drivers of RSLR, particularly sediment supply and deposition, will be a core determinant of long-term sustainability over the next century.

Future changes in the intensity and distribution of hazardous events, which are highly uncertain at the local scale, are also an important driver of future risk trends. Broad evidence suggests that climate change is affecting tropical cyclone intensity and river flooding (11, 29), global sea-level rise is accelerating (12, 30), and local sea-level rise may be substantially different than the global mean in some coastal areas because of regional patterns of ocean heat uptake and glacial isostatic adjustment (30). Land subsidence, taken as constant over time in our study, is also likely to change as future global population

growth occurs predominantly in urban areas (31), driving further anthropogenic change in already stressed deltas. Growth in population, urbanization, and economic development is leading to increased interest in expanding hydropower infrastructure, which is already proliferating across many river systems (32, 33). Expanding hydropower infrastructure will reduce sediment transport and the discharge capacity of river systems that are essential for nourishing deltas (6). Delta shorelines, for instance, are highly sensitive to the balance between sediment supply and absolute wave energy (4).

Future environmental, geophysical, and societal changes will reposition, in many cases considerably, most of the world's deltas into a future space of elevated risk. Although potential geophysical changes require additional research at the regional and local scales, our study demonstrates that economic ability and decisions to deploy engineering solutions will be key factors in
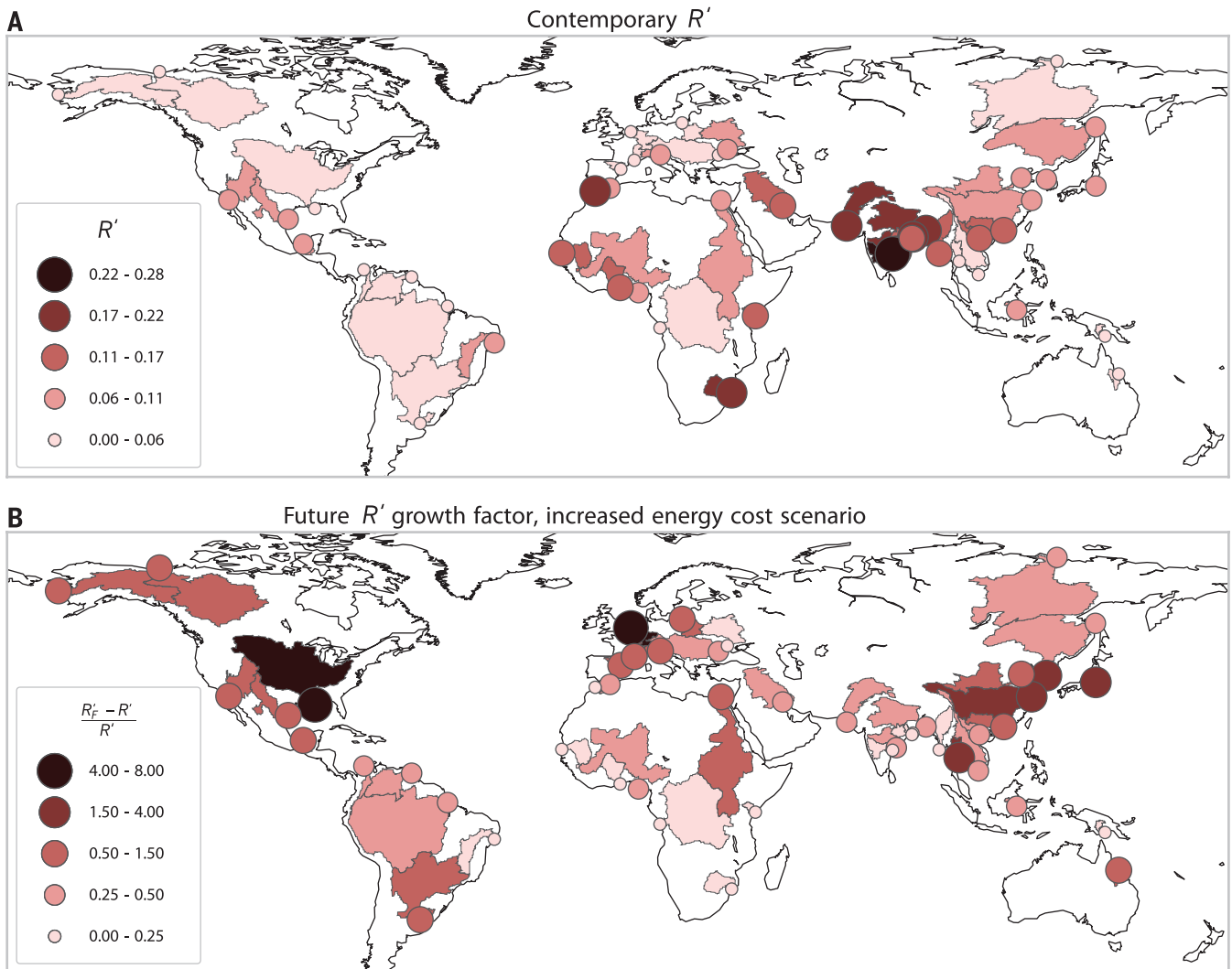

Fig. 4. **Contemporary risk trend and future risk-trend growth.** (**A**) High contemporary values of R' are distributed globally among the highly populated deltas of Southeast Asia and deltas in developing parts of Africa and the Middle East. (**B**) Estimated 50-year growth in the future risk trend, R'_F, relative to the current R'. The highest relative increases in R'_F are in the Rhine, Mississippi, Han, Tone, and Chao Phraya deltas, all systems where current risk is reduced through investments enabled by high GDP and energy costs that are affordable relative to the future scenario.

determining how sustainable deltas become in the long term. Investments that manage the drivers of RSLR, rather than its symptoms, will be necessary to sustain deltas. Although the time horizons are long, acting now is essential, given that rehabilitation will be difficult (if not impossible) to achieve once ground is lost to rising seas.

REFERENCES AND NOTES

1. C. D. Woodroffe, R. J. Nicholls, Y. Saito, Z. Chen, S. L. Goodbred, in *Global Change and Integrated Coastal Management*, N. Harvey, Ed. (Springer Science and Business Media, Dordrecht, Netherlands, 2006), pp. 277–314.
2. M. VanKoningsveld, J. P. M. Mulder, M. J. F. Stive, L. VanDerValk, A. W. VanDerWeck, *J. Coast. Res.* **242**, 367–379 (2008).
3. J. W. Day Jr. *et al.*, *Science* **315**, 1679–1684 (2007).
4. J. P. M. Syvitski, Y. Saito, *Global Planet. Change* **57**, 261–282 (2007).
5. J. P. Ericson, C. J. Vorosmarty, S. L. Dingman, L. G. Ward, M. Meybeck, *Global Planet. Change* **50**, 63–82 (2006).
6. C. J. Vörösmarty *et al.*, *Global Planet. Change* **39**, 169–190 (2003).
7. H. J. Wang *et al.*, *Global Planet. Change* **57**, 331–354 (2007).
8. J. P. M. Syvitski *et al.*, *Nat. Geosci.* **2**, 681–686 (2009).
9. S. Mazzotti, A. Lambert, M. Van der Kooij, A. Mainville, *Geology* **37**, 771–774 (2009).
10. S. Higgins, I. Overeem, A. Tanaka, J. P. M. Syvitski, *Geophys. Res. Lett.* **40**, 3898–3902 (2013).
11. T. R. Knutson *et al.*, *Nat. Geosci.* **3**, 157–163 (2010).
12. B. P. Horton, S. Rahmstorf, S. E. Engelhart, A. C. Kemp, *Quat. Sci. Rev.* **84**, 1–6 (2014).
13. F. G. Renaud *et al.*, *Curr. Opin. Environ. Sustain.* **5**, 644–654 (2013).
14. J. W. Day, M. Moerschbaecher, D. Pimentel, C. Hall, A. Yáñez-Arancibia, *Ecol. Eng.* **65**, 33–48 (2014).
15. S. Temmerman *et al.*, *Nature* **504**, 79–83 (2013).
16. National Research Council, *Landscapes on the Edge: New Horizons for Research on Earth's Surface* (National Academies Press, Washington, DC, 2010).
17. N. Brooks, W. N. Adger, P. M. Kelly, *Glob. Environ. Change* **15**, 151–163 (2005).
18. V. Gornitz, *Palaeogeogr. Palaeoclimatol. Palaeoecol.* **89**, 379–398 (1991).
19. B. S. Halpern *et al.*, *Science* **319**, 948–952 (2008).
20. C. J. Vörösmarty *et al.*, *Nature* **467**, 555–561 (2010).
21. D. L. Balk *et al.*, *Adv. Parasitol.* **62**, 119–156 (2006).
22. S. Cutter, *Prog. Hum. Geogr.* **20**, 529–539 (1996).
23. C. J. Vörösmarty, L. B. de Guenni, W. M. Wollheim, B. Pellerin, D. Bjerklie, M. Cardoso, C. D'Almeida, P. Green, L. Colon, *Philos. Trans. R. Soc. London Ser. A* **371** (2013); http://rsta.royalsocietypublishing.org/content/371/2002/20120408.
24. Y. Budiyono, J. Aerts, J. Brinkman, M. A. Marfai, P. Ward, *Nat. Hazards* **75**, 389–413 (2015).
25. Y. C. E. Yang, P. A. Ray, C. M. Brown, A. F. Khalil, W. H. Yu, *Nat. Hazards* **75**, 2773–2791 (2015).
26. T. Bucx, M. Marchand, B. Makaske, C. van de Guchte, *Comparative Assessment of the Vulnerability and Resilience of 10 Deltas − Synthesis Report* (Delta Alliance report number 1, Delta Alliance International, Delft-Wageningen, Netherlands, 2010).
27. P. Kabat *et al.*, *Nat. Geosci.* **2**, 450–452 (2009).
28. U.S. Energy Information Administration, *Annual Energy Outlook 2015* (DOE/EIA-0383, U.S. Department of Energy, Washington, DC, 2015).
29. R. Dankers *et al.*, *Proc. Natl. Acad. Sci. U.S.A.* **111**, 3257–3261 (2014).
30. S. Jevrejeva, J. C. Moore, A. Grinsted, A. P. Matthews, G. Spada, *Global Planet. Change* **113**, 11–22 (2014).
31. K. C. Seto, B. Güneralp, L. R. Hutyra, *Proc. Natl. Acad. Sci. U.S.A.* **109**, 16083–16088 (2012).
32. C. Kuenzer *et al.*, *Sustain. Sci.* **8**, 565–584 (2013).
33. C. Zarfl, A. E. Lumsdon, J. Berlekamp, K. Tydecks, K. Tockner, *Aquat. Sci.* **77**, 161–170 (2015).

HUMORAL IMMUNITY

T cell help controls the speed of the cell cycle in germinal center B cells

Alexander D. Gitlin,[1] Christian T. Mayer,[1] Thiago Y. Oliveira,[1] Ziv Shulman,[1] Mathew J. K. Jones,[2] Amnon Koren,[4] Michel C. Nussenzweig[1,3]*

The germinal center (GC) is a microanatomical compartment wherein high-affinity antibody-producing B cells are selectively expanded. B cells proliferate and mutate their antibody genes in the dark zone (DZ) of the GC and are then selected by T cells in the light zone (LZ) on the basis of affinity. Here, we show that T cell help regulates the speed of cell cycle phase transitions and DNA replication of GC B cells. Genome sequencing and single-molecule analyses revealed that T cell help shortens S phase by regulating replication fork progression, while preserving the relative order of replication origin activation. Thus, high-affinity GC B cells are selected by a mechanism that involves prolonged dwell time in the DZ where selected cells undergo accelerated cell cycles.

Antibodies elicited during T cell–dependent immune responses undergo substantial increases in affinity over time (*1*). This phenomenon, known as affinity maturation, takes place in the germinal center (GC), where antigen-specific B cells diversify their antibodies by somatic hypermutation (*2*) and undergo selective clonal expansion (*3–7*). Together, these events are essential to the development of effective antibody responses.

GC B cells bearing antibody variants with higher affinity are selectively expanded during iterative rounds of migration between the dark zone (DZ), where they proliferate and hypermutate, and the light zone (LZ), where they capture antigen displayed on the surface of follicular dendritic cells (*8–11*). By binding and internalizing more antigen in the LZ, high-affinity clones present more peptide–major histocompatibility complex II (MHCII) and thereby elicit greater help from CD4+ T follicular helper cells (*11, 12*). The magnitude of T cell help determines how long B cells reside in the DZ, which provides selected cells more time to proliferate and expand in between rounds of competition in the LZ (*13*). Whether this mechanism alone explains how high-affinity B cells are selected remains unknown.

To explore additional mechanisms that could contribute to selection, we used an adoptive transfer model in which antigen presentation by a subset of GC B cells can be acutely and selectively increased (*11, 14, 15*). B cells carrying a knock-in antigen receptor specific for the hapten 4-hydroxy-3-nitrophenylacetyl (NP) (B1-8hi) were transferred into ovalbumin (OVA)–primed wild-type mice that were boosted with NP-OVA. Whereas the majority of transferred B1-8hi B cells were DEC205−/− (~85%), a subset (~15%) of the B1-8hi B cells were DEC205+/+ (*10, 16*). DEC205 is an endocytic receptor expressed by GC B cells that delivers antigen to MHCII processing compartments (*14*). Targeting DEC205 with an antibody that is fused at its C terminus to OVA (αDEC–OVA), but not the irrelevant control antigen *Plasmodium falciparum* circumsporozoite protein (αDEC-CS) (*17*), increases the amount of cognate peptide–MHCII displayed on the surface of B1-8hi DEC205+/+ GC B cells, which leads to their selective expansion (*11–13*).

To determine whether B cells receiving high levels of T cell help show a specific change in gene expression, we compared DZ cells in the G_1 phase of the cell cycle from αDEC-OVA– and control αDEC-CS–treated GCs, using a fluorescent ubiquitination-based cell cycle indicator (Fuccitg) (fig. S1) (*18, 19*). RNA sequencing revealed that T cell–mediated selection produced a statistically significant increase in gene expression programs associated with the cell cycle, metabolism (including the metabolism of nucleotides), and genes downstream of c-Myc and the E2F transcription factors (Fig. 1, A and B, and fig. S2). Finding an

[1]Laboratory of Molecular Immunology, The Rockefeller University, New York, NY 10065, USA. [2]Molecular Biology Program, Memorial Sloan-Kettering Cancer Center, 1275 York Avenue, New York, NY 10065, USA. [3]Howard Hughes Medical Institute (HHMI), The Rockefeller University, New York, NY 10065, USA. [4]Department of Genetics, Harvard Medical School, Boston, MA 02115, USA.
*Corresponding author. E-mail: nussen@rockefeller.edu

Science

AAAS
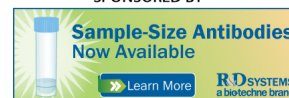
Profiling risk and sustainability in coastal deltas of the world
Z. D. Tessler *et al.*
Science **349**, 638 (2015);
DOI: 10.1126/science.aab3574